Main Manuscript for

The androgen receptor in mesenchymal progenitors regulates skeletal muscle mass via *Igf1* expression in male mice.

Hiroshi Sakai[1,2,*], Hideaki Uno[2], Harumi Yamakawa[2], Kaori Tanaka[3], Aoi Ikedo[1], Akiyoshi Uezumi[4], Yasuyuki Ohkawa[3], Yuuki Imai[1,2,*]

[1]Division of Integrative Pathophysiology, Proteo-Science Center, Ehime University, Toon, Ehime 791-0295, Japan.

[2]Department of Pathophysiology, Ehime University Graduate School of Medicine, Toon, Ehime 791-0295, Japan.

[3]Division of Transcriptomics, Medical Institute of Bioregulation, Kyushu University, Higashi-ku, Fukuoka 812-0054, Japan.

[4]Divison of Cell Heterogeneity, Medical Institute of Bioregulation, Kyushu University, Higashi-ku, Fukuoka 812-0054, Japan.

[*]Hiroshi Sakai, Yuuki Imai

Hiroshi Sakai, DVM, PhD, and Yuuki Imai, MD, PhD, Proteo-Science Center, Graduate School of Medicine, Ehime University, Shitsukawa, Toon, Ehime, 791-0295, Japan.

+81-89-960-5925

Email: sakai.hiroshi.wh@ehime-u.ac.jp (H.S.), y-imai@m.ehime-u.ac.jp (Y.I.)

Preprint servers: We have posted the manuscript on bioRxiv (https://doi.org/10.1101/2023.11.21.568190).

Author Contributions: Conceptualization, H.S. and Y.I.; Methodology, H.S., H.U., K.T., A.I., A.U., Y.O., and Y.I.; Software, H.S., H.U., and K.T.; Investigation, H.S., H.U., H.Y., K.T., and A.I.; Writing – Original Draft, H.S. and Y.I.; Writing – Review & Editing, H.S. and Y.I.; Funding Acquisition, H.S. and Y.I.; Resources, H.S., K.T., A.U., Y.O., and Y.I.; Supervision, H.S. and Y.I.

Competing Interest Statement: The authors declare no competing interests.

Classification: Biological Sciences, Medical Sciences

Keywords: androgen receptor, skeletal muscle, mesenchymal progenitors, Igf1

This PDF file includes:

Main Text

Figures 1 to 4

Abstract

Androgens exert their effects primarily by binding to the androgen receptor (AR), a ligand-dependent nuclear receptor. While androgens have anabolic effects on skeletal muscle, previous studies reported that AR functions in myofibers to regulate skeletal muscle quality, rather than skeletal muscle mass. Therefore, the anabolic effects of androgens are exerted via extra-myofiber cells or tissues. In this context, the cellular and molecular mechanisms of AR in mesenchymal progenitors, which play a crucial role in maintaining skeletal muscle homeostasis, remain largely unknown. In this study, we demonstrated expression of AR in mesenchymal progenitors and found that targeted AR ablation in mesenchymal progenitors reduced limb muscle mass in mature adult, but not young or aged, male mice, although fatty infiltration of muscle was not affected. The absence of AR in mesenchymal progenitors led to remarkable perineal muscle hypotrophy, regardless of age, due to abnormal regulation of transcripts associated with apoptosis and extracellular matrix organization. Additionally, we revealed that AR in mesenchymal progenitors regulates the expression of insulin-like growth factor 1, which can increase skeletal muscle mass in a paracrine manner. These findings indicate that the anabolic effects of androgens regulate skeletal muscle mass via, at least in part, AR signaling in mesenchymal progenitors.

61 **Significance statement**

62 Androgens are essential not only for the development of male sexual characteristics but also for a
63 range of physiological functions, including the regulation of skeletal muscle growth and
64 function. Understanding the functionality of the androgen receptor (AR) is essential for
65 comprehending the mechanisms through which androgens exert their effects on skeletal muscles,
66 as these effects are mediated through AR binding. Our study demonstrates that AR is expressed
67 in mesenchymal progenitors, which play a vital role in muscle homeostasis, and regulates the
68 expression of insulin-like growth factor 1 (Igf1)—a key player in skeletal muscle growth—to
69 control muscle mass. Our study provides significant insights into potential therapeutic strategies
70 for addressing muscle atrophy conditions like sarcopenia.

Main Text

Introduction

Androgens are crucial regulators of various biological processes, including the development and maintenance of male characteristics. Notably, in a physiological context, the administration of androgens or androgen analogs has been shown to exert anabolic effects on muscles, resulting in increased muscle mass, strength, and body weight (1, 2). These physiological effects are mediated by activation of the androgen receptor (AR), a member of the nuclear receptor superfamily (3). However, despite that clinical administration of androgens in men can successfully increase skeletal muscle mass (4), the precise cellular and molecular mechanisms underlying the function of AR in muscle remain largely unexplored.

Skeletal muscle represents a complex tissue comprising multiple cell types, and the effects of androgens are likely mediated by various cell populations expressing AR within skeletal muscles. While male mice systemically lacking AR exhibit low skeletal muscle strength and mass, similar to female levels (5), we previously showed that muscle hypertrophy can be induced by androgen administration even in the absence of AR in muscle fibers, suggesting that non-myofiber AR contributes to the regulation of muscle mass (6). Furthermore, another of our studies demonstrated that deletion of AR in satellite cells, which are muscle stem cells responsible for muscle regeneration, had a limited effect on their proliferation and differentiation (7). Additionally, since limb muscle mass remains unaffected even in mice with AR ablation in both myofibers and muscle stem cells (8), other cells expressing AR within the muscles may play a role in regulating skeletal muscle mass.

Mesenchymal progenitors (9), also known as fibro/adipogenic progenitors (10), have been identified as a cell population distinct from myogenic cells characterized by the expression

94 of platelet-derived growth factor receptor alpha (PDGFRα). These cells are involved in the
95 maintenance and regeneration of skeletal muscle (11, 12). Conversely, mesenchymal progenitors
96 have been implicated in pathological fibrosis and fat accumulation in skeletal muscle (13). AR
97 expression has been reported in cells located in the interstitium or outside the basal lamina in
98 both mouse and human skeletal muscles (14, 15). Additionally, ablation of AR specifically in
99 embryonic cells of the mesenchyme led to impaired development of the perineal levator ani (LA)
100 and bulbocavernosus (BC) muscles (16), which are particularly responsive to androgen.
101 Furthermore, the reduced proliferation of undifferentiated myoblasts in these mutant mice
102 suggested a potential paracrine regulatory role of mesenchymal AR in controlling skeletal
103 muscles (16). Despite this knowledge, the specific role of AR in adult mesenchymal progenitors
104 in skeletal muscles remains unexplored.
105 Here we investigate the role of AR expressed in mesenchymal progenitors in muscle
106 maintenance using mice with mesenchymal progenitor-specific AR ablation. We show that AR
107 in mesenchymal progenitors plays a critical role in maintaining skeletal muscle mass via
108 regulation of insulin-like growth factor 1 (Igf1) expression in male mice.

Results

AR ablation in mesenchymal progenitors was validated in *PDGFRα-CreER;AR$^{L2/Y}$* mice

AR expression in fibroblasts of the perineal LA muscles and in mesenchymal cells of the fetal LA muscles has been reported (14, 16, 17); however, it is unknown whether mesenchymal progenitors in adult limb muscle express AR. To examine the expression pattern of AR in mesenchymal progenitors, immunofluorescence staining of PDGFRα, a marker of mesenchymal progenitors (9), and AR was performed in adult (12 weeks old) male mice. We found that AR was expressed in mesenchymal progenitors staining positive for PDGFRα (Fig. 1A), as well as in muscle fibers surrounded by laminin-expressing basal lamina, consistent with previous findings (17, 18).

To investigate the role of AR in mesenchymal progenitors, *PDGFRα-CreER* (19) and *AR$^{L2/Y}$* (20) mice were crossed to selectively delete the AR gene in mesenchymal progenitors expressing PDGFRα. Tamoxifen (TMX) was administered to Cre control male mice (*PDGFRα-CreER*) and mutant male mice (*PDGFRα-CreER;AR$^{L2/Y}$*) for 5 consecutive days to induce AR ablation (Fig. 1B). To assess the efficiency of AR ablation, immunofluorescence staining of PDGFRα and AR was performed in control and mutant mice. Quantification of PDGFRα and AR expression in forelimb biceps brachii (BB) and hindlimb tibialis anterior (TA) muscles demonstrated a significant decrease of 90% in AR protein in mutant mice compared with control mice, confirming successful ablation of AR expression in mesenchymal progenitors from *PDGFRα-CreER;AR$^{L2/Y}$* mice (Fig. 1C). In contrast, loss of AR in mesenchymal progenitors did not affect the number of PDGFRα+ cells (Fig. S1A). Taken together, these findings demonstrate successful and specific loss of AR expression in PDGFRα+ cells, rendering them an optimal model for investigating AR in mesenchymal progenitors in skeletal muscles.

132

133 **Lack of AR in mesenchymal progenitors had a limited effect on steady-state limb skeletal**
134 **muscles**

135 Because ablation of PDGFRα+ cells in intact muscles results in skeletal muscle atrophy (11, 12),
136 we first analyzed the muscles of control and mutant mice under steady-state conditions at a
137 young age (14 weeks old) (Fig. 1B). Body weight and limb skeletal muscle mass were not
138 affected in mutant compared with control mice at 2 weeks after TMX administration (Fig. S1B).
139 Moreover, the grip strength of mutant mice was comparable with that of control mice (Fig. S1C).
140 The minimum Ferret diameter, which is the robust parameter in order to measure myofiber size,
141 and number of myofibers in BB and TA muscles remained unchanged in mutant mice (Fig. S1D,
142 E). As relayed signaling between mesenchymal progenitors and muscle stem (satellite) cells is
143 critical for muscle hypertrophy (21), we also quantified the number of muscle stem cells.
144 Immunofluorescence staining of Pax7, a marker of muscle stem cells (22), revealed no difference
145 in the number of muscle stem cells between control and mutant BB and TA muscles (Fig. S1F).
146 We next investigated the fiber types of slow soleus muscles, which are affected by muscle fiber-
147 and muscle stem cell-specific AR ablation (8, 23). Analysis of soleus muscles fiber types by
148 immunofluorescence staining of type I (Myh7), type IIa (Myh2), and type IIx (without signals)
149 muscle fibers demonstrated no difference in the fiber-type parameters (minimum Ferret diameter
150 and frequency of each fiber-type) between control and mutant mice (Fig. S1G, H). Thus, AR
151 expression loss in mesenchymal progenitors has a limited effect on the steady-state limb muscles
152 of young mice.

153

154 **The impact of AR deficiency in mesenchymal progenitors on adipogenesis in muscles was**
155 **limited**

156 We also examined the adipogenesis of mesenchymal progenitors in mutant mice because
157 adipocytes originate from mesenchymal progenitors in skeletal muscles (9). To address this, both
158 the control and mutant mice were subjected to an 8-week regimen of high fat diet (HFD) feeding
159 (Fig. S2A). No significant differences were observed between the control mice and mutant mice
160 in terms of total body weight, hindlimb muscle weights, epididymal white adipose tissue
161 (eWAT) mass, and subcutaneous white adipose tissue (sWAT) mass (Fig. S2B), and grip
162 strength (Fig. S2C). Immunofluorescence staining of perilipin, a marker of adipocytes (24),
163 along with laminin, demonstrated no significant difference in the minimum Ferret diameter of
164 myofibers or the area occupied by adipocytes between the control and mutant TA muscles (Fig.
165 S2D, E).

166 To further investigate the impact of AR deficiency in muscle adipogenesis, we employed
167 a muscle injury model by administering glycerol injections into the TA muscle of both control
168 and mutant mice (Fig. S2F). No significant differences were observed between the control and
169 mutant mice in terms of the body and TA muscle weights at 2 weeks after injection (Fig. S2G).
170 Immunofluorescence staining of perilipin in conjunction with laminin (Fig. S2H) revealed no
171 significant difference in the minimum Ferret diameter of myofibers or the area occupied by
172 adipocytes between the control and mutant TA muscles (Fig. S2I). These findings suggest that
173 the absence of AR in mesenchymal progenitors does not significantly affect the adipogenic
174 properties of TA muscles.
175

176 **AR deficiency in mesenchymal progenitors affected limb skeletal muscles in mature adult**
177 **but not aged mice**
178 To investigate the effect of the duration of AR ablation on mesenchymal progenitors, we
179 analyzed mature adult (6 months old) mice and compared the Cre control group and mutant
180 group (Fig. 2A). In the mature adult mutant mice, we observed decreases in body weight, TA,
181 and gastrocnemius muscle weights (Fig. 2B), while there were no significant changes in the
182 weights of eWAT and sWAT (Fig. 2B), which are affected by systemic AR ablation (25).
183 However, grip strength (Fig. 2C) was comparable between the control and mutant mice.
184 Additionally, the weights of the entire body, hindlimb muscles, and white adipose tissues
185 were compared between aged (28 months old) control and mutant mice (Fig S2J). The aged
186 mutant mice did not exhibit any significant differences from the aged control mice (Fig. S2K and
187 S2L). Therefore, our findings demonstrate that AR deficiency in mesenchymal progenitors
188 affects skeletal muscle mass in mature adult mice only, not young or aged mice, primarily in the
189 limbs.
190
191 **Mesenchymal progenitor-specific AR ablation induced atrophy of LA/BC muscles**
192 The perineal LA/BC skeletal muscle complex exhibits increased responsiveness to androgens
193 compared with other striated muscles (26). Because this perineal muscle complex also has higher
194 AR expression (14), we examined the impact of AR ablation on mesenchymal progenitors of
195 LA/BC skeletal muscles. We confirmed efficient ablation of AR in PDGFRα+ cells in LA
196 muscles as well as limb muscles (Fig. 2D, E). We also found that AR depletion in mesenchymal
197 progenitors in LA muscles led to a decrease in the number of PDGFRα+ cells (Fig. 2F). At 14
198 weeks, 6 months, and 28 months of age, the LA/BC mass was consistently lower in the mutant

199 mice than control mice (Fig. 2G). Because AR ablation in myofibers using a promoter region
200 derived from the human α-skeletal actin (HSA) gene (*HSA-Cre;AR*$^{L2/Y}$ mice) also leads to
201 reduced LA/BC mass (27), we generated *HSA-Cre;PDGFRα-CreER;AR*$^{L2/Y}$ mice to examine
202 whether the weight reduction depended on AR in myofibers. Interestingly, the LA/BC weight
203 was lower in *HSA-Cre;AR*$^{L2/Y}$ mice than in *PDGFRα-CreER;AR*$^{L2/Y}$ mice (Fig. 2H). Moreover,
204 *HSA-Cre;PDGFRα-CreER;AR*$^{L2/Y}$ mice had the lowest LA/BC mass compared with *HSA-*
205 *Cre;AR*$^{L2/Y}$ and *PDGFRα-CreER;AR*$^{L2/Y}$ mice (Fig. 2G). These findings suggest that AR
206 expression in both myofibers and mesenchymal progenitors independently regulates the mass of
207 perineal muscles. Examination of the cross-sectional area of LA muscles by laminin staining
208 (Fig. 2I) revealed a lower myofiber size and fewer myofibers in the mutant mice than control
209 mice (Fig. 2J). In summary, AR expression in mesenchymal progenitors independently regulates
210 the mass of perineal muscles, separate from its influence on myofibers.
211
212 **AR regulated genes related to extracellular matrix organization in mesenchymal**
213 **progenitors**
214 To determine the effects of AR on gene expression, we performed RNA-seq in PDGFRα+ cells
215 from the LA/BC muscles of both control and mutant mice (Fig. 3A). Using a previously
216 established gating strategy for isolating mesenchymal progenitors (CD45− CD31− Vcam1−
217 PDGFRα+) (12) (Fig. S3A), we isolated 300 PDGFRα+ cells from LA/BC muscles for RNA-
218 seq. We detected more than 100,000 genes in these cells, indicating sufficient read depth for
219 further analysis (Fig. S3B). The principal component analysis (PCA) plot showed separation
220 between the control and mutant samples (Fig. S3C). We identified 80 upregulated and 76
221 downregulated genes, including AR, in PDGFRα+ cells from the mutant mice (Fig. S3D). The

222 upregulated genes were enriched in the Gene Ontology (GO) terms including regulation of cell
223 death and cell motility (Fig. 3B). On the other hand, the downregulated genes were enriched in
224 the GO terms related to extracellular matrix (ECM) organization and regulation of proteolysis
225 (Fig. 3C).

226 To determine the AR target genes, we used CUT&RUN method for AR and trimethylated
227 lysine 4 from histone H3 (H3K4me3), which is enrich in active promoters, in mesenchymal
228 progenitors isolated from C57BL/6J male mice (Fig 3D), at 2 hours after treatment with
229 dihydrotestosterone (DHT), which was confirmed to induce AR expression in skeletal muscles
230 (Fig. S3E, S3F). We detected total 6542 peaks of AR in mesenchymal progenitors in skeletal
231 muscles. The AR peaks were primarily distributed in intron or intergenic regions (Fig. S3G),
232 similar to previous reports with AR ChIP-seq in muscle and non-muscle tissues (28, 29). We also
233 found the androgen response elements (ARE) in these peaks as the most enriched motif as well
234 as AR half-site (Fig. 3E, S3H). Moreover, AR CUT&RUN was validated by peaks found in the
235 *Fkbp5* locus (Fig. S3I), where canonical AR binding sites are located for several tissues (28). By
236 profiling AR peaks with AR and H3K4me3 reads, we found that AR binding sites were present
237 mainly not in promoter region (Fig. 3F). Furthermore, AR binding events were enriched for
238 regulation of locomotion and ECM organization GO terms (Fig. 3G). These results indicate that
239 AR in mesenchymal progenitors directly regulate the transcriptions including ECM organization
240 genes.

241

242 **AR in mesenchymal progenitors regulated *Igf1* expression**

243 To further investigate the gene regulation by AR in mesenchymal progenitors, we combined the
244 RNA-seq and CUT&RUN analysis. We found 39 genes which were downregulated in AR-

245 deficient mesenchymal progenitors and have AR peaks annotated by a nearest transcription start
246 sites (TSS) analysis (Fig. 4A). Top enriched GO term of these genes was ECM organization (Fig.
247 4B), including Collagen family (*Col1a1*, *Col3a1*, *Col4a1*, *Col4a2*, *Col5a1*, *Col5a2*, and *Col6a2*,
248 Fig. S4A and S4B), and *Igf1* (Fig. 4C), which is critical for maintaining muscle mass (30). We
249 also found the bindings of AR with ARE and peaks of H3K4me3 in upstream of *Igf1* TSS (Fig.
250 4D). Moreover, AR peaks were found with ARE in *Ar* gene locus (Fig. S4C), indicating the
251 regulation of *Ar* by AR in mesenchymal progenitors as other cells (31). To further investigate the
252 effects of androgen and AR on *Igf1* expression, we isolated PDGFRα+ cells from C57BL/6J
253 male mice treated with DHT (Fig. 4E). *Igf1* expression was upregulated in PDGFRα+ cells after
254 DHT administration (Fig. 4F). We also found reduction of IGF1 protein in the mutant LA
255 muscles (Fig. 4G and 4H). Finally, to determine whether the reduction in muscle mass in the
256 mutant mice was due to decreased IGF1 protein, we injected recombinant IGF1 into the LA/BC
257 muscles of the mutant mice just before TMX administration (Fig. 4I). We found that the mass of
258 the LA/BC muscles in IGF1-treated mutant mice increased compared to saline-injected mutant
259 mice, reaching levels comparable to those of saline-injected control mice (Fig. 4J). This finding
260 indicates that IGF1 injection effectively prevents the weight loss of LA/BC muscles in mutant
261 mice. Taken together, AR in mesenchymal progenitors regulates *Igf1* expression controlling
262 skeletal muscle mass.

263 **Discussion**

264 In the present study, we demonstrated that male mice with specific AR ablation in mesenchymal
265 progenitors showed lower skeletal muscle mass in the limbs only at the mature adult stage, but
266 not at a younger stage (14 weeks old). Taken together with previous report demonstrating that
267 mice with AR ablation specifically in fast-twitch fibers lack muscle mass reduction at 13 weeks
268 old but exhibit this reduction at 12–13 months old (23), there may be an effect that requires time
269 to develop. Additionally, we demonstrated that the number of Pax7+ muscle stem cells was
270 similar between adult control and mutant mice. This is in contrast to the observed reduction in
271 myoblast proliferation following deletion of AR in the mesenchyme of BC muscles during
272 development (16), providing evidence that AR in mesenchymal progenitors plays distinct roles
273 during development, adulthood, and aging in mice. We also showed that specific ablation of AR
274 in mesenchymal progenitors does not affect the fiber types of slow-twitch muscles. Depletion of
275 mesenchymal progenitors results in a slight increase in the proportion of slow fibers (type I)
276 predominantly in fast-twitch TA muscles (12), suggesting that factors other than AR in
277 mesenchymal progenitors influence muscle fiber types. Muscle strength was either unaffected or
278 only slightly affected in myofiber-specific AR ablation mice (32), suggesting that non-myogenic
279 cells expressing AR may play a role in mediating muscle strength. However, grip strengths for
280 forelimbs were not affected in the mutant mice in all experimental groups conducted in present
281 study. Because the conventional grip strength test is influenced by various factors, including
282 inconsistent procedures and the motivation of the mice (33), more sensitive methods for
283 assessing muscle function, such as measuring in situ maximum isometric torque, and active and
284 passive force in skinned fibers (34), could detect subtle differences in muscle strength in the
285 mutant mice.

286 PDGFRα+ cells are the origin of ectopic adipocytes in skeletal muscles (9, 10). However,
287 the specific molecular mechanisms underlying fatty infiltration of muscles remain largely
288 unexplored (35). In general, androgen and AR signaling seem to have inhibitory effects on
289 adipogenesis (36). Serum androgens are linked to reduced levels of fatty infiltration of skeletal
290 muscles (37). In contrast, deprivation of androgens leads to an increase in fatty infiltration of
291 skeletal muscle in men (38). Moreover, transgenic mice expressing AR induced by collagen type
292 I alpha 1, which is also expressed in mesenchymal progenitors (39), have reduced body weight
293 and fat mass (40). Additionally, HFD-induced fat mass deposition in skeletal muscles was
294 increased by a low androgen level caused by orchidectomy (41). However, our results indicate
295 that AR deficiency in mesenchymal progenitors does not affect adipogenesis in skeletal muscle
296 even after HFD feeding or glycerol injection. An indirect androgen pathway may also regulate
297 adipogenesis of mesenchymal progenitors in skeletal muscles. Indeed, recent research indicates
298 that androgens can modulate macrophage polarization, subsequently affecting adipocyte
299 differentiation (42). Further studies are needed to gain a comprehensive understanding of the
300 mechanisms by which androgens and AR signaling influence fatty infiltration of muscle.
301 We observed a modest reduction in the muscle weight of the mutant mice at the mature
302 adult age (24 weeks old), but this effect was not observed in aged mice (28 months old). Because
303 selective ablation of AR in myofibers does not lead to reduced muscle mass even in 40-week-old
304 mice (27), the role of AR in mesenchymal progenitors is more important than its role in
305 myofibers in the context of muscle maintenance, at least at the mature adult age. The timing of
306 AR ablation could impact skeletal muscle mass, given the variation in initiation times for AR
307 ablation (tamoxifen treatment at 12 weeks old for analysis at 14 and 24 weeks, and at 8 weeks
308 old for analysis at 28 months). Experiments involving AR ablation at different ages, such as

309 TMX treatment at young (12 weeks old), mature adult (24 weeks old) and aged (24 months old)
310 mice, would help to clarify whether these results are influenced by age or the duration of AR
311 ablation. A decrease in testosterone concentration, even in 1-year-old mice compared with young
312 12-week-old mice (43), may contribute to muscle mass loss, potentially masking any subtle
313 differences between the aged control and mutant mice. Due to the reduction in muscle mass
314 observed in 2-year-old mice with AR depletion specifically in fast-twitch fibers (23), AR
315 expression in muscle fibers may play a crucial role in regulating muscle metabolism and quality,
316 which help maintain muscle mass in aged mice.

317 The perineal skeletal muscles LA and BC are highly androgen sensitive. Muscle fiber-
318 specific AR knockout results in a more pronounced mass reduction in LA/BC muscles compared
319 with limb muscles (26, 27), which is consistent with our present study demonstrating a consistent
320 reduction in LA/BC muscles in mice with AR ablation in mesenchymal progenitors. We also
321 demonstrated that AR deficiency in mesenchymal progenitors resulted in reduced LA/BC
322 weight, although the extent of the reduction was milder compared with mice in which AR was
323 ablated in muscle fibers. Furthermore, the double Cre mice (*HSA-Cre;PDGFRα-CreER;AR*$^{L2/Y}$),
324 with ablation of AR in both myofibers and mesenchymal progenitors, exhibited a greater
325 reduction in LA/BC mass compared with single Cre mice (*HSA-Cre;AR*$^{L2/Y}$ or *PDGFRα-*
326 *CreER;AR*$^{L2/Y}$). Overexpression of AR in skeletal muscle fibers using HSA promoter (44, 45)
327 does not rescue the atrophy of LA muscles of testicular feminization mutation (*Ar*^{Tfm}) male rat
328 (45), supporting a separate role of AR in mesenchymal progenitors for maintaing perineal muslce
329 mass. Taken together, AR expression in mesenchymal progenitors independently regulates the
330 mass of perineal muscles, separate from the influence of AR in myofibers. The distinct reactions
331 observed in perineal and limb muscles could be attributed to a greater abundance of myonuclei

332 expressing AR in perineal muscles compared with limb muscles (14). Nevertheless, our findings
333 revealed that the majority of PDGFRα+ cells exhibited AR expression in both limb and perineal
334 muscles, suggesting an additional mechanism by which AR in mesenchymal progenitors
335 regulates muscle mass and other mesenchymal progenitor functions.

336 We also found that several ECM genes, including members of the collagen family, were
337 downregulated in AR-deficient mesenchymal progenitors, with AR peaks identified by a nearest
338 TSS analysis. These ECM components are primarily produced by PDGFRα+ cells in both
339 healthy and fibrotic skeletal muscles (39). AR expression promotes fibrosis in the heart, kidney,
340 and ovary (46–48), indicating that androgen/AR signaling governs ECM remodeling. Moreover,
341 downregulation of AR in PDGFRα+ fibroblasts from squamous cell carcinomas induces the
342 activation of cancer-associated fibroblasts (CAF), which remodel the ECM within the tumor
343 microenvironment (49). This suggests a general role for AR in PDGFRα+ cells under both
344 physiological and pathological conditions. Given that muscle diseases involving ECM
345 remodeling, such as muscular dystrophy and sarcopenia, are often accompanied by muscle
346 atrophy (50), it is plausible that ECM reduction due to AR deficiency contributes to skeletal
347 muscle atrophy. Further studies are needed to elucidate the relationship between AR, ECM, and
348 skeletal muscle plasticity.

349 The signaling pathway involving IGF1 plays a crucial role in both the developmental
350 growth and steady-state maintenance of skeletal muscle mass (51, 52). IGF1 is produced
351 primarily in the liver (53) but local production, including in skeletal muscles, is induced by
352 androgen treatment. The administration of testosterone to older men led to an increase in IGF1
353 protein expression in the limb (vastus lateralis) muscles (54). *Igf1* expression is decreased in the
354 LA/BC muscles of mice with skeletal muscle-specific AR ablation (27). Dubois et al. has

355 reported indirect androgen regulation of IGF1 via non myocytic AR because Myod-Cre-driven
356 AR-deficient mice showed no reduction in the *Igf1* transcript level, and *Igf1* expression was
357 decreased after castration in skeletal muscles (17). We demonstrated that AR in mesenchymal
358 progenitors in skeletal muscles regulated *Igf1* expression, governing muscle mass. Moreover,
359 activation of Akt signaling via the expression of Bmp3b in mesenchymal progenitors (12)
360 suggests a connection with Igf1, highlighting the complex interplay of signaling pathways in the
361 maintenance of skeletal muscle mass.

362 A limitation of our study in that we focused on male mice for studying AR in
363 mesenchymal progenitors of skeletal muscles. Because serum levels of androgens, including
364 testosterone and DHT, are also measurable in female mice (43), androgen/AR signaling could
365 potentially affect female skeletal muscles as well. Furthermore, *AR* was not differentially
366 expressed between males and females of human skeletal muscles (55), indicating potential roles
367 of AR in female skeletal muscles. On the other hand, genomic AR knockout mice show impaired
368 skeletal muscle development and function in males, but not females (5). Although muscle fiber-
369 specific AR knockout in female mice limitedly impacted on the expression of transcripts (6) and
370 muscle mass (23), more comparative work between male and female mice will be necessary to
371 determine whether AR plays important roles in female mesenchymal progenitors, as the function
372 of AR in these cells may differ from its role in female skeletal muscle fibers.

373 In summary, our results show that AR in mesenchymal progenitors regulates skeletal
374 muscle mass via *Igf1* expression (Fig. 4K). Further investigations into the limb muscles of aged
375 mice and humans are required to confirm whether combined treatment with androgens and IGF1
376 could be effective in treating muscle atrophy conditions such as sarcopenia.

377 **Materials and Methods**

378 **Animals**

379 *PDGFRα-CreER* mice (19), *HSA-Cre* mice (56), and C57BL/6J male mice were purchased from
380 Jackson Laboratories (Strain #: 018280, 006149, and 000664, respectively). $AR^{L2/Y}$ mice have
381 been described (20). *PDGFRα-CreER* male mice were crossed with $AR^{L2/+}$ female mice to
382 generate *PDGFRα-CreER;*$AR^{L2/Y}$ male mutant mice. Male littermates with the *PDGFRα-*
383 *CreER;*$AR^{+/Y}$ genotype were used as control mice. To generate *HSA-Cre;PDGFRα-CreER;*$AR^{L2/Y}$
384 male mice, *HSA-Cre* male mice were crossed with *PDGFRα-CreER;*$AR^{L2/+}$ female mice. All
385 mice were housed in a specific pathogen-free facility under climate-controlled conditions and a
386 12-hour light/dark cycle and were provided water and a standard diet *ad libitum*. In both control
387 and mutant mice, 100 μL of 20 mg/mL tamoxifen (TMX, Sigma-Aldrich, Cat# T5648),
388 dissolved in corn oil (Sigma-Aldrich, Cat# C8267), was injected intraperitoneally for 5
389 consecutive days at 8 or 12 weeks of age. A high-fat diet (HFD, CLEA Japan, Cat# HFD32) was
390 given *ad libitum* for 8 weeks to induce obesity in mice. The diet was refreshed every 2 days. To
391 induce fatty infiltration of skeletal muscle, 100 μL of 50% v/v glycerol was injected into tibialis
392 anterior (TA) muscles under anesthesia using isoflurane (57). To induce AR signaling, vehicle
393 (Veh) or dihydrotestosterone (DHT or stanolone, 2.5 mg/mouse; Tokyo Chemical Industry, Cat#
394 A0462), dissolved in absolute ethanol and diluted in 0.3% w/v hydroxypropyl cellulose (Wako,
395 Cat# 085-07932) in PBS, was injected subcutaneously into C57BL/6J male mice at 2 hours
396 before sampling. In *PDGFRα-CreER;*$AR^{L2/Y}$ male mutant mice, 10 μg/50 μL of recombinant
397 IGF1 (PeproTech, Cat# AF-100-11) dissolved in saline (Otsuka, Cat# 3311401A2026) or 50 μL
398 of saline was injected directly into LA/BC muscles for 4 consecutive days at 12 weeks of age.
399 The same amount of saline was injected into LA/BC muscles of male littermates with the

400 *PDGFRα-CreER;AR*$^{+/Y}$ genotype for the control. TMX (100 μL of 20 mg/mL) was injected
401 intraperitoneally, just after injection of IGF1 or saline, for 4 consecutive days. All animal
402 experiments were approved by the Animal Experiment Committee of Ehime University
403 (Approval No. 37A1-1·16) and were conducted in full compliance with the Guidelines for
404 Animal Experiments at Ehime University.
405
406 **Grip strength**
407 The grip strength of the forelimb was measured using a strain gauge (Melquest, Cat# GPM-
408 100B). The maximal force was determined after 10 measurements. The mean value recorded by
409 two independent experimenters was reported as the grip strength of each mouse.
410
411 **Immunofluorescence staining and microscopy**
412 For immunofluorescence staining, muscles were snap frozen in liquid nitrogen-chilled
413 isopentane. Cryosections of 10 μm thickness were prepared for immunofluorescence staining.
414 Sections were fixed in 4% paraformaldehyde in PBS for 5 min, blocked in 5% goat serum
415 (Gibco, Cat# 16210-064) in PBS for 60 min, and incubated with primary antibodies overnight at
416 4°C. For staining of myosin heavy chain (Myh), sections were air-dried and blocked with
417 M.O.M. reagent (Vector Laboratories, Cat# MKB-2213-1) at room temperature for 60 min.
418 Primary antibodies for Myh diluted in 1% BSA/PBS were incubated at 37°C for 45 min. The
419 antibodies used for immunofluorescence staining were anti-AR (Abcam, Cat# ab108341,
420 RRID:AB_10865716; 1/100), anti-PDGFRA (R&D Systems, Cat# AF1062,
421 RRID:AB_2236897; 1/80), anti-Laminin α2 (Santa Cruz Biotechnology, Cat# sc-59854,
422 RRID:AB_784266; 1/400), anti-Pax7 (DSHB, Cat# PAX7, RRID:AB_528428; 1/5), anti-

423 Laminin (Sigma-Aldrich, Cat# L9393, RRID:AB_477163; 1/500), anti-Myh7 (DSHB, Cat# BA-
424 D5, RRID:AB_2235587, supernatant; 1/100), anti-Myh2 (DSHB, Cat# SC-71,
425 RRID:AB_2147165, supernatant; 1/100), anti-Perilipin (Sigma-Aldrich, Cat# P1873,
426 RRID:AB_532267; 1/250), Alexa fluor 488 goat anti-rabbit IgG (Thermo Fisher Scientific, Cat#
427 A-11008; RRID:AB_143165; 1/1000), Alexa fluor 555 donkey anti-goat IgG (Thermo Fisher
428 Scientific, Cat# A-21432, RRID:AB_2535853; 1/1000), Alexa fluor 647 goat anti-rat IgG
429 (Thermo Fisher Scientific, Cat# A-21247, RRID:AB_141778; 1/1000), Alexa fluor 568 goat
430 anti-mouse IgG1 (Thermo Fisher Scientific, Cat# A-21124, RRID: AB_2535766; 1/1000), Alexa
431 fluor 488 goat anti-mouse IgG2b (Thermo Fisher Scientific, Cat# A-21141, RRID:AB_2535778;
432 1/1000), Alexa fluor 568 goat anti-rabbit IgG (Thermo Fisher Scientific, Cat# A-11011,
433 RRID:AB_143157; 1/1000), and Alexa fluor 647 goat anti-rabbit IgG (Thermo Fisher Scientific,
434 Cat# A27040; RRID:AB_143165; 1/1000). Nuclei were counterstained with DAPI. Entire cross
435 sections of fluorescence images were photographed using BIOREVO (Keyence) or Axio
436 Observer7 (Zeiss).
437
438 **Quantification of muscle sections**
439 To quantify the number, cross-sectional area (CSA), and minimum Ferret diameter of the
440 myofibers, captured images of entire cross sections were analyzed using Fiji (v2.3.0)
441 (https://imagej.net/Fiji). The myofiber area was identified by the laminin+ signals. The region of
442 interest (ROI) was set within the laminin+ areas. The frequency of each muscle fiber type in the
443 ROI was recorded by Trainable Weka Segmentation in Fiji after manual training. Small (< 150
444 μm^2) or large (> 10,000 μm^2) fibers were excluded for analyzing. The number of AR+PDGFRα+

445 mesenchymal progenitors, Pax7+ satellite cells, and the perilipin+ area was manually counted or
446 measured using Fiji.
447
448 **Isolation of mesenchymal progenitors from skeletal muscle**
449 Isolation of mononuclear cells from muscle was performed as described previously (58) with
450 minor modifications. Briefly, muscles were chopped in PBS on ice and digested using 800 U/mL
451 collagenase type 2 (Worthington, Cat# LS004177) in F10 medium (Gibco, Cat# 11550-043)
452 supplemented with 10% horse serum (Gibco, Cat# 26050-088) and antibiotic–antimycotic
453 (Gibco, Cat# 15240-062) for 60 min. Another digestion was conducted using 1000 U/mL
454 collagenase type 2 and 11 U/mL dispase (Gibco, Cat# 17105-041) for 30 min. The supernatants
455 were transferred to a 40 μm cell strainer (Falcon, Cat# 352340) to filter the debris and then
456 centrifuged to yield a cell suspension. The following antibodies were used: FITC anti-CD31
457 (BioLegend, Cat# 102406; RRID:AB_312901; 1/100), FITC anti-CD45 (BioLegend, Cat#
458 103108, RRID:AB_312973; 1/100), PE anti-VCAM1 (Thermo Fisher Scientific, Cat# 12-1061-
459 82, RRID:AB_2572573; 1/100), and APC anti-PDGFRα (R&D Systems, Cat# FAB1062A,
460 RRID:AB_3073817; 1/30). The BD FACSAria II (RRID:SCR_018091) or BD FACSAria
461 Fusion (BD Biosciences) was used for fluorescence-activated cell sorting (FACS), and the plot
462 was analyzed by FlowJo v10.1r7 (BD Life Sciences, RRID:SCR_008520).
463
464 **RNA-seq and data analysis**
465 For isolation of RNA from mesenchymal progenitors in LA/BC muscles, 300 PDGFRα+ cells
466 were sorted into the wells of a 96-well plate containing 10 μL lysis buffer at 4°C. The lysis
467 buffer was prepared by mixing 1 μL RNase inhibitor (Takara, Cat# 2313A) and 19 μL 10X lysis

468 buffer (Takara, Cat# 635013) diluted to 1X with nuclease-free water. 3' UTR RNA-seq was
469 conducted using the CEL-Seq2 protocol (59), with the exception of employing the Second Strand
470 Synthesis Module (New England Biolabs, Cat# E6111L) for double-stranded cDNA synthesis.
471 The library was then amplified via 10 cycles of PCR without any sample pooling. Subsequently,
472 the library was sequenced on the Illumina NovaSeq 6000, and quantitative analysis was
473 performed using 81 bp of insert reads (Read2).
474 Cell barcode and UMI information from Read1 were extracted using UMI-tools (v1.1.2)
475 (60) with the following command: "umi_tools extract -I read1.fastq --read2-in=read2.fastq --bc-
476 pattern=NNNNNNNNNNCCCCCCCCC". Adaptor and low-quality sequences were removed,
477 and reads with a length less than 20 bp were discarded using TrimGalore (v0.6.7;
478 http://www.bioinformatics.babraham.ac.uk/projects/trim_galore/). The processed reads were then
479 mapped to the GRCm38 reference genome using HISAT2 (v2.2.1) (61). Read counts for each
480 gene were obtained using featureCounts (v2.0.1) (62), and UMI duplications were removed
481 using UMI-tools. Four cell barcodes, "ATGCAATGC," "GACACGACA," "CGATGCGAT,"
482 and "TCTGGTCTG," were assigned to each sample. Differentially expressed genes were
483 identified using DESeq2 (v1.36.0) (63) with thresholds of |log2FC| > 1 and padj < 0.1.
484 Metascape (64) was used for Gene Ontology (GO) enrichment analysis.
485
486 **CUT&RUN and data analysis**
487 C57BL/6J male mice (10-12 weeks old) were treated with DHT at 2 hours before sampling for
488 FACS. For isolation of chromatin from mesenchymal progenitors in hindlimbs muscles, 500,000
489 PDGFRα+ cells were sorted to 20%FBS, DMEM/F12 (Gibco, Cat# 10565-018), Ultroser G
490 (Pall, Cat# 15950-017) supplemented with DHT (100 nM) to activate AR signaling during

491 sorting. After sorting, the nuclei were prepared with ChIC/CUT&RUN Assay Kit (Active Motif,
492 Cat# 53180) following the manufacturer's protocol. For AR (n = 4), H3K4me3 (n = 2), and IgG
493 control (n = 2) CUT&RUN, the following antibodies (1 μg/reaction) were used: anti-AR
494 (Abcam, Cat# ab108341, RRID:AB_10865716), anti-H3K4me3 (Active Motif, Cat# 39916,
495 RRID:AB_2687512), and rabbit negative control IgG (Active Motif, part of Cat# 53180). To
496 obtain enriched DNA after the CUT&RUN reaction, 20 μL of DNA purification elution buffer
497 was used instead of 55. The library was prepared using NEBNext Ultra II for DNA Library
498 Preparation for Illumina (New England Biolabs, Cat# E7645L) with some modifications
499 according to the Active Motif's instruction. All reactions were performed by half volume.
500 Constructed libraries were analyzed by 2100 Bioanalyzer using High Sensitivity DNA kit
501 (Agilent Technologies, Cat# 5067-4626), and quantified by qPCR using KAPA Library
502 Quantification Kits (Kapa Biosystems, Cat# KK4824). The library was sequenced on the
503 Illumina NovaSeq 6000 for 51 cycles of paired-end sequencing.
504 Paired-end reads were trimmed with TrimGalore and mapped to mm10 using Bowtie2
505 (v2.4.5) (65) with the following options: --no-mixed --no-discordant. Multi or no mate reads
506 were removed with samtools (v1.10) (66) view (-q 4 -F 0x2). To identify AR peaks across
507 samples, BAM files were merged across biological replicates (n = 2) to call peaks with MACS2
508 (v2.2.7.1) (-q 0.05) (67). H3K4me3 peaks were called on individual BAM files using MACS2 (-
509 q 0.0001). Merged BAM files for AR and IgG were used for downstream analysis (2 merged
510 BAM files for AR and 1 merged BAM file for IgG). Motif enrichment analysis of AR peaks was
511 performed with HOMER (v4.11) (68) findMotifs with -size 200 -mask options and AR peaks
512 were annotated to mm10 genes using annotatePeaks (-size 200 -mask) from MACS2 summit
513 files. Peaks distribution was annotated on mm10 (TxDb.Mmusculus.UCSC.mm10.knownGene,

514 R package version 3.4.7.) using ChIPpeakAnno package (v3.30.1) (69, 70) with MACS2
515 narrowPeak files. Promoter region was defined as 2000 bp upstream to 500 bp downstream of
516 transcription start sites (TSS). Common AR peaks-associated genes between replicates were
517 identified with Venn diagrams tools (http://bioinformatics.psb.ugent.be/webtools/Venn/). GO
518 enrichment analysis of common AR peaks-associated genes for GO Biological Process was
519 performed with Metascape. To generate bigwig files, merged (AR or IgG) or individual
520 (H3K4me3) BAM files were converted to CPM-normalized bigwig files using deepTools
521 (v3.5.1) (71) bamCoverage (--binSize 100 --normalizeUsing CPM). Peaks were visualized using
522 Integrative Genomics Viewer (IGV, v2.12.3) (72) with bigwig files. A count matrix for
523 aggregation plot was generated by deepTools computeMatrix reference-point (--skipZeros) with
524 AR and H3K4me3 bigwig files. Heatmaps were generated with count matrix files using
525 deepTools plotHeatmap.
526
527 **RNA isolation and quantitative real-time PCR**
528 C57BL/6J male mice (12 weeks old) were treated with Veh or DHT at 2 hours before sampling
529 for FACS, as described above. Total RNA was extracted from freshly sorted 30,000 PDGFRα+
530 cells from LA/BC muscles using the RNeasy Plus Micro Kit (Qiagen, Cat# 74034) following the
531 manufacturer's protocol. Reverse transcription was performed using PrimeScript (Takara, Cat#
532 RR036A) to synthesize cDNA from total RNA. Quantitative PCR (qPCR) was conducted in
533 technical duplicate samples utilizing TB Green Premix Ex Taq II (Takara, Cat# RR820S) and the
534 Thermal Cycler Dice (Takara, Cat# TP850). The expression levels of the target genes were
535 normalized to that of *Rpl13a*. The primer sequences are listed in Table S1.
536

537 **Western blotting**

538 LA muscles were dissolved in RIPA buffer (Fujifilm, Cat# 182-02451) supplemented with
539 protease inhibitors (Nacalai Tesque, Cat# 25955-11). Tissue-extracts were separated by SDS-
540 PAGE and transferred to polyvinylidene fluoride membranes. The membranes were blocked with
541 5% skim milk in TBS with Tween-20 (PBST), followed by incubation with anti-IGF1 (R&D
542 Systems, Cat# AF791, RRID:AB_2248752; 1/2000) or anti-GAPDH antibodies (Cell Signaling
543 Technology, Cat# 5174, RRID: AB_10622025; 1/1000) overnight at 4°C. The membranes were
544 incubated with an anti-goat (Agilent, Cat# P0160, 1:5000) or anti-rabbit immunoglobulin/HRP
545 secondary antibody (Agilent, Cat# P0448, RRID: AB_2617138; 1:5000) for 60 min at room
546 temperature. Signals were detected using ECL Prime Western Blotting Detection Reagents
547 (Amersham, Cat# RPN2232) on the Image Quant LAS 4000 system (GE Healthcare). Band
548 images were quantified by Fiji.

549

550 **Statistical analysis**

551 Prism 9 (GraphPad Software) or R (v4.0.5) (https://www.r-project.org) was used for the
552 statistical analysis. Welch's t-test was used to compare two groups. The two-sample test for
553 equality of proportions was performed using the test of equal or given proportions. To compare
554 variables among three or more groups, Brown-Forsythe and Welch's ANOVA test with
555 Dunnett's T3 multiple comparison test was used.

556 **Acknowledgments and funding sources**

557 We are grateful to A. Nishio and Y. Sato for their technical support. We thank Y. Tanaka for the
558 flow cytometry support, N. Tokunaga for the library preparations, and other members of the
559 Division of Medical Research Support, the Advanced Research Support Center, Ehime
560 University. This study was partly performed in the Cooperative Research Project Program in the
561 Medical Institute of Bioregulation (MIB), Kyushu University. We also thank the Medical
562 Research Center for High Depth Omics, MIB, Kyushu University for the sequencing, and RIST
563 at Kyushu University for the high-performance computing. This work was supported in part by
564 MEXT/JSPS KAKENHI (JP21K17568 to H.S.; JP22H03203 to Y.I.) and the HIRAKU-Global
565 Program, which is funded by MEXT's "Strategic Professional Development Program for Young
566 Researchers" and Takeda Science Foundation (to H.S.).

567 **Data Availability**

568 RNA-seq and CUT&RUN data have been deposited and are publicly available in the Gene

569 Expression Omnibus as accession number GSE247378.

570 **References**

571

572 1. G. N. Papanicolaou, E. A. Falk, General Muscular Hypertrophy Induced by Androgenic
573 Hormone. *Science* **87**, 238–239 (1938).

574 2. S. Bhasin, *et al.*, The Effects of Supraphysiologic Doses of Testosterone on Muscle Size and
575 Strength in Normal Men. *N. Engl. J. Med.* **335**, 1–7 (1996).

576 3. D. B. Lubahn, *et al.*, Cloning of Human Androgen Receptor Complementary DNA and
577 Localization to the X Chromosome. *Science* **240**, 327–330 (1988).

578 4. A. M. Lincoff, *et al.*, Cardiovascular Safety of Testosterone-Replacement Therapy. *N. Engl. J.*
579 *Med.* **389**, 107–117 (2023).

580 5. H. E. MacLean, *et al.*, Impaired skeletal muscle development and function in male, but not
581 female, genomic androgen receptor knockout mice. *FASEB J.* **22**, 2676–2689 (2008).

582 6. I. Sakakibara, *et al.*, Myofiber androgen receptor increases muscle strength mediated by a
583 skeletal muscle splicing variant of Mylk4. *iScience* **24**, 102303 (2021).

584 7. H. Sakai, T. Sato, M. Kanagawa, S. Fukada, Y. Imai, Androgen receptor in satellite cells is not
585 essential for muscle regenerations. *Exp. Results* **1** (2020).

586 8. V. Dubois, *et al.*, A satellite cell-specific knockout of the androgen receptor reveals myostatin
587 as a direct androgen target in skeletal muscle. *FASEB J.* **28**, 2979–2994 (2014).

588 9. A. Uezumi, S. Fukada, N. Yamamoto, S. Takeda, K. Tsuchida, Mesenchymal progenitors
589 distinct from satellite cells contribute to ectopic fat cell formation in skeletal muscle. *Nat. Cell*
590 *Biol.* **12**, 143–152 (2010).

591 10. A. W. B. Joe, *et al.*, Muscle injury activates resident fibro/adipogenic progenitors that
592 facilitate myogenesis. *Nat. Cell Biol.* **12**, 153–163 (2010).

593 11. M. N. Wosczyna, *et al.*, Mesenchymal Stromal Cells Are Required for Regeneration and
594 Homeostatic Maintenance of Skeletal Muscle. *Cell Rep.* **27**, 2029-2035.e5 (2019).

595 12. A. Uezumi, *et al.*, Mesenchymal Bmp3b expression maintains skeletal muscle integrity and
596 decreases in age-related sarcopenia. *J. Clin. Investig.* **131** (2020).

597 13. A. Uezumi, *et al.*, Fibrosis and adipogenesis originate from a common mesenchymal
598 progenitor in skeletal muscle. *J. Cell Sci.* **124**, 3654–3664 (2011).

599 14. J. A. Johansen, S. M. Breedlove, C. L. Jordan, Androgen Receptor Expression in the Levator
600 Ani Muscle of Male Mice. *J. Neuroendocr.* **19**, 823–826 (2007).

601 15. I. Sinha-Hikim, W. E. Taylor, N. F. Gonzalez-Cadavid, W. Zheng, S. Bhasin, Androgen
602 Receptor in Human Skeletal Muscle and Cultured Muscle Satellite Cells: Up-Regulation by
603 Androgen Treatment. *J. Clin. Endocrinol. Metab.* **89**, 5245–5255 (2004).

604 16. L. A. Ipulan, *et al.*, Nonmyocytic Androgen Receptor Regulates the Sexually Dimorphic
605 Development of the Embryonic Bulbocavernosus Muscle. *Endocrinology* **155**, 2467–2479
606 (2014).

607 17. V. Dubois, *et al.*, Enobosarm (GTx-024) Modulates Adult Skeletal Muscle Mass
608 Independently of the Androgen Receptor in the Satellite Cell Lineage. *Endocrinology* **156**, 4522–
609 4533 (2015).

610 18. M. Kanou, *et al.*, Polyamine pathway is associated with muscle anabolic effects by androgen
611 receptor ligand. *JCSM Rapid Commun.* **4**, 57–74 (2021).

612 19. S. H. Kang, M. Fukaya, J. K. Yang, J. D. Rothstein, D. E. Bergles, NG2+ CNS Glial
613 Progenitors Remain Committed to the Oligodendrocyte Lineage in Postnatal Life and following
614 Neurodegeneration. *Neuron* **68**, 668–681 (2010).

615 20. T. Matsumoto, K. Takeyama, T. Sato, S. Kato, Androgen receptor functions from reverse
616 genetic models. *J. Steroid Biochem. Mol. Biol.* **85**, 95–99 (2003).

617 21. A. Kaneshige, *et al.*, Relayed signaling between mesenchymal progenitors and muscle stem
618 cells ensures adaptive stem cell response to increased mechanical load. *Cell Stem Cell* **29**, 265-
619 280.e6 (2022).

620 22. P. Seale, *et al.*, Pax7 Is Required for the Specification of Myogenic Satellite Cells. *Cell* **102**,
621 777–786 (2000).

622 23. T. Hosoi, *et al.*, Sarcopenia phenotype and impaired muscle function in male mice with fast-
623 twitch muscle-specific knockout of the androgen receptor. *Proc. Natl. Acad. Sci.* **120**,
624 e2218032120 (2023).

625 24. A. S. Greenberg, *et al.*, Perilipin, a major hormonally regulated adipocyte-specific
626 phosphoprotein associated with the periphery of lipid storage droplets. *J. Biol. Chem.* **266**,
627 11341–11346 (1991).

628 25. W. Fan, *et al.*, Androgen Receptor Null Male Mice Develop Late-Onset Obesity Caused by
629 Decreased Energy Expenditure and Lipolytic Activity but Show Normal Insulin Sensitivity With
630 High Adiponectin Secretion. *Diabetes* **54**, 1000–1008 (2005).

631 26. J. Ophoff, *et al.*, Androgen Signaling in Myocytes Contributes to the Maintenance of Muscle
632 Mass and Fiber Type Regulation But Not to Muscle Strength or Fatigue. *Endocrinology* **150**,
633 3558–3566 (2009).

634 27. C. Chambon, *et al.*, Myocytic androgen receptor controls the strength but not the mass of
635 limb muscles. *Proc. Natl. Acad. Sci.* **107**, 14327–14332 (2010).

636 28. P. Pihlajamaa, *et al.*, Tissue-specific pioneer factors associate with androgen receptor
637 cistromes and transcription programs. *EMBO J.* **33**, 312–326 (2014).

638 29. K. Ghaibour, *et al.*, Androgen receptor coordinates muscle metabolic and contractile
639 functions. *J. Cachexia, Sarcopenia Muscle* **14**, 1707–1720 (2023).

640 30. C. Rommel, *et al.*, Mediation of IGF-1-induced skeletal myotube hypertrophy by
641 PI(3)K/Akt/mTOR and PI(3)K/Akt/GSK3 pathways. *Nat. Cell Biol.* **3**, 1009–1013 (2001).

642 31. J. M. Grad, L. S. Lyons, D. M. Robins, K. L. Burnstein, The Androgen Receptor (AR)
643 Amino-Terminus Imposes Androgen-Specific Regulation of AR Gene Expression via an Exonic
644 Enhancer. *Endocrinology* **142**, 1107–1116 (2001).

645 32. F. Jardí, *et al.*, Androgen and estrogen actions on male physical activity: a story beyond
646 muscle. *J. Endocrinol.* **238**, R31–R52 (2018).

647 33. H. Takeshita, *et al.*, Modified forelimb grip strength test detects aging-associated
648 physiological decline in skeletal muscle function in male mice. *Sci. Rep.* **7**, 42323 (2017).

649 34. T. Yamada, Y. Ashida, D. Tatebayashi, K. Himori, Myofibrillar function differs markedly
650 between denervated and dexamethasone-treated rat skeletal muscles: Role of mechanical load.
651 *PLoS ONE* **14**, e0223551 (2019).

652 35. M. W. Hamrick, M. E. McGee-Lawrence, D. M. Frechette, Fatty Infiltration of Skeletal
653 Muscle: Mechanisms and Comparisons with Bone Marrow Adiposity. *Front. Endocrinol.* **7**, 69
654 (2016).

655 36. J. Rizk, R. Sahu, D. Duteil, An overview on androgen-mediated actions in skeletal muscle
656 and adipose tissue. *Steroids* **199**, 109306 (2023).

657 37. I. Miljkovic, *et al.*, Bioactive androgens and glucuronidated androgen metabolites are
658 associated with subcutaneous and ectopic skeletal muscle adiposity among older black men.
659 *Metabolism* **60**, 1178–1185 (2011).

660 38. D. Chang, *et al.*, Androgen deprivation muscle attenuation. *J. Méd. Imaging Radiat. Oncol.*
661 **58**, 223–228 (2014).

662 39. M. A. Chapman, K. Mukund, S. Subramaniam, D. Brenner, R. L. Lieber, Three distinct cell
663 populations express extracellular matrix proteins and increase in number during skeletal muscle
664 fibrosis. *Am. J. Physiol. Cell Physiol.* **312**, C131–C143 (2017).

665 40. A. A. Semirale, X. Zhang, K. M. Wiren, Body composition changes and inhibition of fat
666 development in vivo implicates androgen in regulation of stem cell lineage allocation. *J. Cell.*
667 *Biochem.* **112**, 1773–1786 (2011).

668 41. V. Dubois, *et al.*, Androgen Deficiency Exacerbates High-Fat Diet-Induced Metabolic
669 Alterations in Male Mice. *Endocrinology* **157**, 648–665 (2016).

670 42. X. Ren, *et al.*, Testosterone regulates 3T3-L1 pre-adipocyte differentiation and epididymal
671 fat accumulation in mice through modulating macrophage polarization. *Biochem. Pharmacol.*
672 **140**, 73–88 (2017).

673 43. M. E. Nilsson, *et al.*, Measurement of a Comprehensive Sex Steroid Profile in Rodent Serum
674 by High-Sensitive Gas Chromatography-Tandem Mass Spectrometry. *Endocrinology* **156**, 2492–
675 2502 (2015).

676 44. D. A. Monks, *et al.*, Overexpression of wild-type androgen receptor in muscle recapitulates
677 polyglutamine disease. *Proc. Natl. Acad. Sci.* **104**, 18259–18264 (2007).

678 45. L. Niel, *et al.*, Sexual Differentiation of the Spinal Nucleus of the Bulbocavernosus Is Not
679 Mediated Solely by Androgen Receptors in Muscle Fibers. *Endocrinology* **150**, 3207–3213
680 (2009).

681 46. Y. Wang, *et al.*, Androgen receptor regulates cardiac fibrosis in mice with experimental
682 autoimmune myocarditis by increasing microRNA-125b expression. *Biochem. Biophys. Res.*
683 *Commun.* **506**, 130–136 (2018).

684 47. S. Allam, *et al.*, Androgen receptor blockade by flutamide down-regulates renal fibrosis,
685 inflammation, and apoptosis pathways in male rats. *Life Sci.* **323**, 121697 (2023).

686 48. D. Wang, *et al.*, Bromodomain-containing protein 4 activates androgen receptor transcription
687 and promotes ovarian fibrosis in PCOS. *Cell Rep.* **42**, 113090 (2023).

688 49. A. Clocchiatti, *et al.*, Androgen receptor functions as transcriptional repressor of cancer-
689 associated fibroblast activation. *J. Clin. Investig.* **128**, 5531–5548 (2018).

690 50. O. Contreras, F. M. V. Rossi, M. Theret, Origins, potency, and heterogeneity of skeletal
691 muscle fibro-adipogenic progenitors—time for new definitions. *Skelet. Muscle* **11**, 16 (2021).

692 51. B. T. O'Neill, *et al.*, Insulin and IGF-1 receptors regulate FoxO-mediated signaling in muscle
693 proteostasis. *J. Clin. Invest.* **126**, 3433–3446 (2016).

694 52. F. Ascenzi, *et al.*, Effects of IGF-1 isoforms on muscle growth and sarcopenia. *Aging Cell*
695 **18**, e12954 (2019).

696 53. R. D. Kineman, M. del Rio-Moreno, A. Sarmento-Cabral, 40 YEARS of IGF1:
697 Understanding the tissue-specific roles of IGF1/IGF1R in regulating metabolism using the
698 Cre/loxP system. *J. Mol. Endocrinol.* **61**, T187–T198 (2018).

699 54. A. A. Ferrando, *et al.*, Testosterone administration to older men improves muscle function:
700 molecular and physiological mechanisms. *Am. J. Physiol. Endocrinol. Metab.* **282**, E601–E607
701 (2002).

702 55. C. M. Lopes-Ramos, *et al.*, Sex Differences in Gene Expression and Regulatory Networks
703 across 29 Human Tissues. *Cell Rep.* **31**, 107795 (2020).

704 56. P. Miniou, *et al.*, Gene targeting restricted to mouse striated muscle lineage. *Nucleic Acids*
705 *Res.* **27**, e27–e30 (1999).

706 57. N. Arsic, *et al.*, Vascular endothelial growth factor stimulates skeletal muscle regeneration in
707 Vivo. *Mol. Ther.* **10**, 844–854 (2004).

708 58. L. Liu, T. H. Cheung, G. W. Charville, T. A. Rando, Isolation of skeletal muscle stem cells
709 by fluorescence-activated cell sorting. *Nat. Protoc.* **10**, 1612–1624 (2015).

710 59. T. Hashimshony, *et al.*, CEL-Seq2: sensitive highly-multiplexed single-cell RNA-Seq.
711 *Genome Biol.* **17**, 77 (2016).

712 60. T. Smith, A. Heger, I. Sudbery, UMI-tools: modeling sequencing errors in Unique Molecular
713 Identifiers to improve quantification accuracy. *Genome Res.* **27**, 491–499 (2017).

714 61. D. Kim, J. M. Paggi, C. Park, C. Bennett, S. L. Salzberg, Graph-based genome alignment and
715 genotyping with HISAT2 and HISAT-genotype. *Nat. Biotechnol.* **37**, 907–915 (2019).

716 62. Y. Liao, G. K. Smyth, W. Shi, featureCounts: an efficient general purpose program for
717 assigning sequence reads to genomic features. *Bioinformatics* **30**, 923–930 (2014).

718 63. M. I. Love, W. Huber, S. Anders, Moderated estimation of fold change and dispersion for
719 RNA-seq data with DESeq2. *Genome Biol.* **15**, 550 (2014).

720 64. Y. Zhou, *et al.*, Metascape provides a biologist-oriented resource for the analysis of systems-
721 level datasets. *Nat. Commun.* **10**, 1523 (2019).

722 65. B. Langmead, S. L. Salzberg, Fast gapped-read alignment with Bowtie 2. *Nat. Methods* **9**,
723 357–359 (2012).

724 66. P. Danecek, *et al.*, Twelve years of SAMtools and BCFtools. *GigaScience* **10**, giab008
725 (2021).

726 67. Y. Zhang, *et al.*, Model-based analysis of ChIP-Seq (MACS). *Genome Biol.* **9**, R137 (2008).

727 68. S. Heinz, *et al.*, Simple Combinations of Lineage-Determining Transcription Factors Prime
728 cis-Regulatory Elements Required for Macrophage and B Cell Identities. *Mol. Cell* **38**, 576–589
729 (2010).

730 69. L. J. Zhu, *et al.*, ChIPpeakAnno: a Bioconductor package to annotate ChIP-seq and ChIP-
731 chip data. *BMC Bioinform.* **11**, 237 (2010).

732 70. L. J. Zhu, Tiling Arrays, Methods and Protocols. *Methods Mol. Biol.* **1067**, 105–124 (2013).

733 71. F. Ramírez, *et al.*, deepTools2: a next generation web server for deep-sequencing data
734 analysis. *Nucleic Acids Res.* **44**, W160–W165 (2016).

735 72. J. T. Robinson, *et al.*, Integrative genomics viewer. *Nat. Biotechnol.* **29**, 24–26 (2011).

736

737

Figures

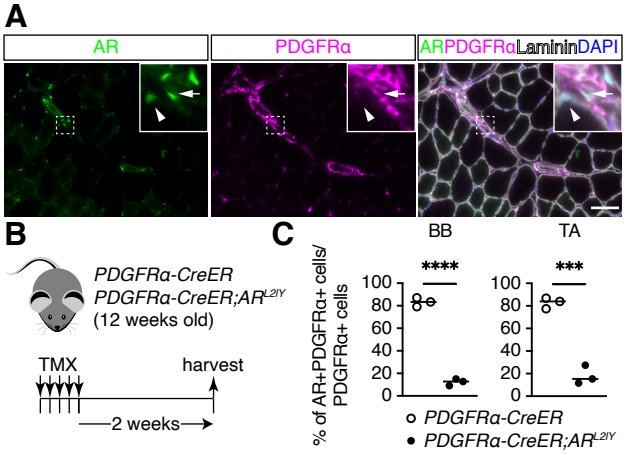

Figure 1. AR ablation in mesenchymal progenitors from *PDGFRα-CreER;AR$^{L2/Y}$* mice. (A) Immunofluorescence staining of AR (left) and PDGFRα (middle) and of both together with laminin and DAPI staining (right) in male TA muscles. Arrows: AR+ and PDGFRα+ cells; arrowheads: AR+ nuclei surrounded by laminin. Scale bar, 50 µm. (B) Experimental design for tamoxifen (TMX) treatment followed by sample harvest. (C) Quantification of AR+ cells among PDGFRα+ cells in the biceps brachii (BB, left) and tibialis anterior (TA, right) muscles of control and mutant mice (n = 3). The two-sample test for equality of proportions: ***$p < 0.001$, ****$p < 0.0001$.

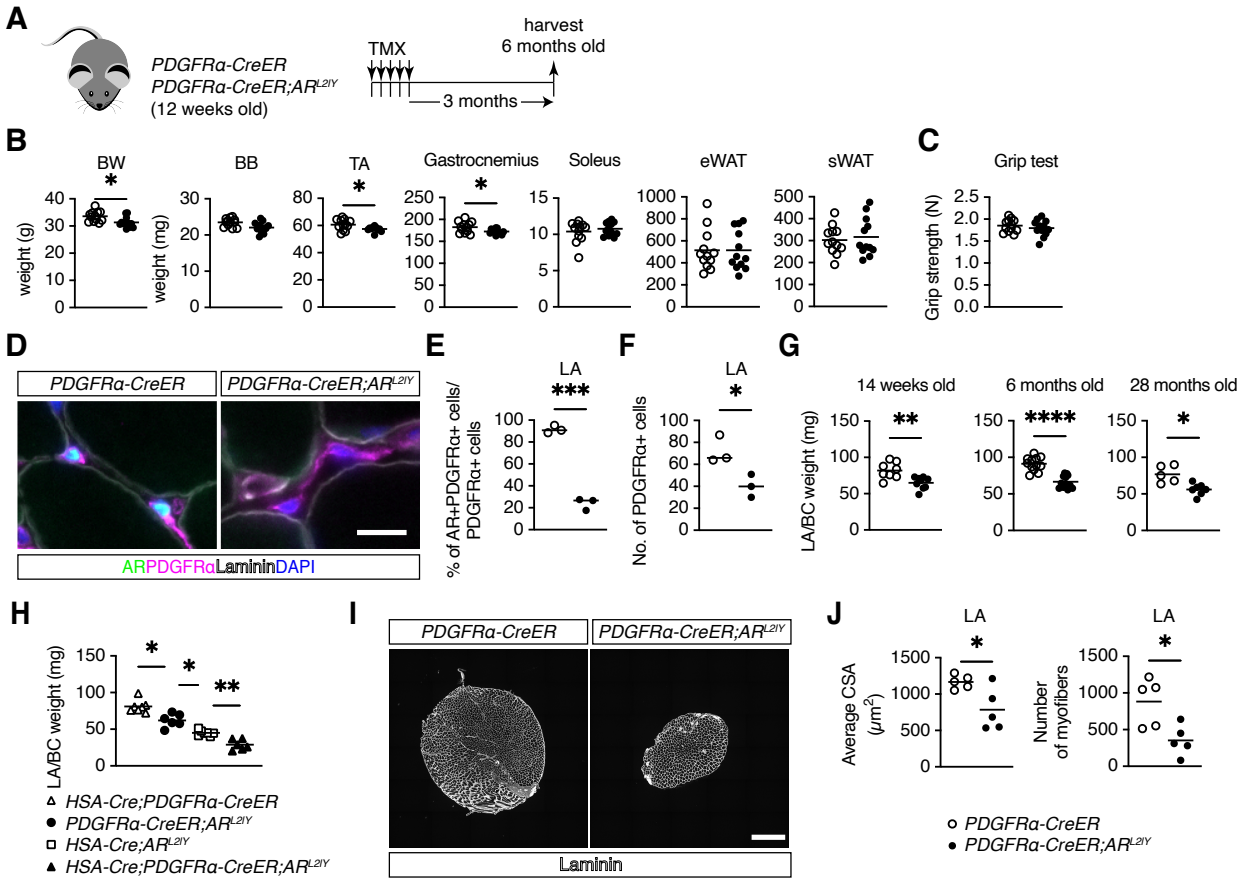

Figure 2. Atrophy of skeletal muscles in mesenchymal progenitor-specific AR-deficient mice. (A) Experimental design for tamoxifen (TMX) treatment followed by sample harvest in mature adult (6 months old) mice. (B and C) Quantification of body weight (BW), muscle mass, epididymal white adipose tissue (eWAT) mass, and subcutaneous WAT (sWAT) mass (B), and grip strength (C) in 6-month-old mice (n = 12). TA, tibialis anterior; BB, biceps brachii. Unpaired t-test with Welch's correction. (D) Immunofluorescence staining of AR, PDGFRα, and laminin with DAPI in levator ani (LA) muscles of control (left) and mutant (right) mice. Scale bar, 10 μm. (E) Quantification of AR+ cells among PDGFRα+ cells in LA muscles of control and mutant mice (n = 3). The two-sample test for equality of proportions. (F) Quantification of PDGFRα+ cells in LA muscles of control and mutant mice (n = 3). Unpaired t-test with Welch's correction. (G) Mass of LA and bulbocavernosus (BC) muscles in 14-week- (n = 8 control; n = 9

760 mutant mice), 6-month- (n = 12), and 28-month-old mice (n = 5 control; n = 7 mutant mice).
761 Unpaired t-test with Welch's correction. (H) Mass of LA/BC muscles in single (*HSA-Cre* or
762 *PDGFRα-CreER*) and double Cre mice. Brown-Forsythe and Welch's ANOVA test with
763 Dunnett's T3 multiple comparison test. (I) Immunofluorescence staining of laminin in LA
764 muscles of control (left) and mutant mice (right). Scale bar, 500 µm. (J) Average cross-sectional
765 area (CSA) (left) and the number of myofibers (right) in control and mutant mice (n = 5).
766 Unpaired t-test with Welch's correction: *$p < 0.05$, **$p < 0.01$, ***$p < 0.001$, ****$p < 0.0001$.

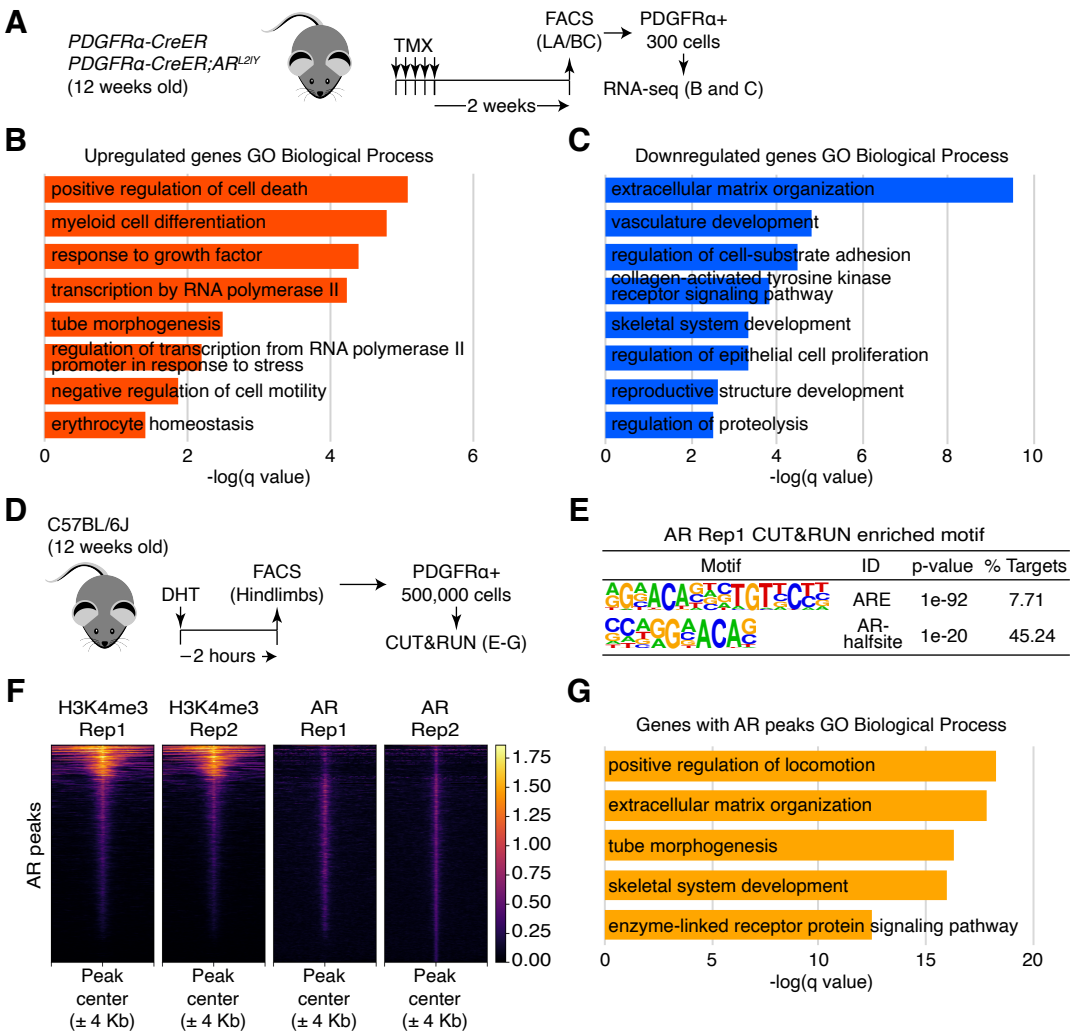

Figure 3. Functional and genomic targets of AR in mesenchymal progenitors of skeletal muscles. (A) Experimental design for tamoxifen (TMX) treatment followed by fluorescence-activated cell sorting (FACS) from levator ani and bulbocavernosus (LA/BC) muscles for RNA-seq. (B and C) Top Gene Ontology (GO) Biological Process terms associated with the upregulated (B) and downregulated (C) genes in PDGFRα+ cells from mutant mice. (D) Experimental design for dihydrotestosterone (DHT) treatment followed by FACS and CUT&RUN. (E) Enriched motifs within AR CUT&RUN peaks. (F) Heatmaps of mean H3K4me3 and AR CUT&RUN counts per million (CPM) normalized read coverage around AR

776 CUT&RUN peaks for individual replicates. (G) Top GO Biological Process terms enriched

777 within AR CUT&RUN peak-associated genes.

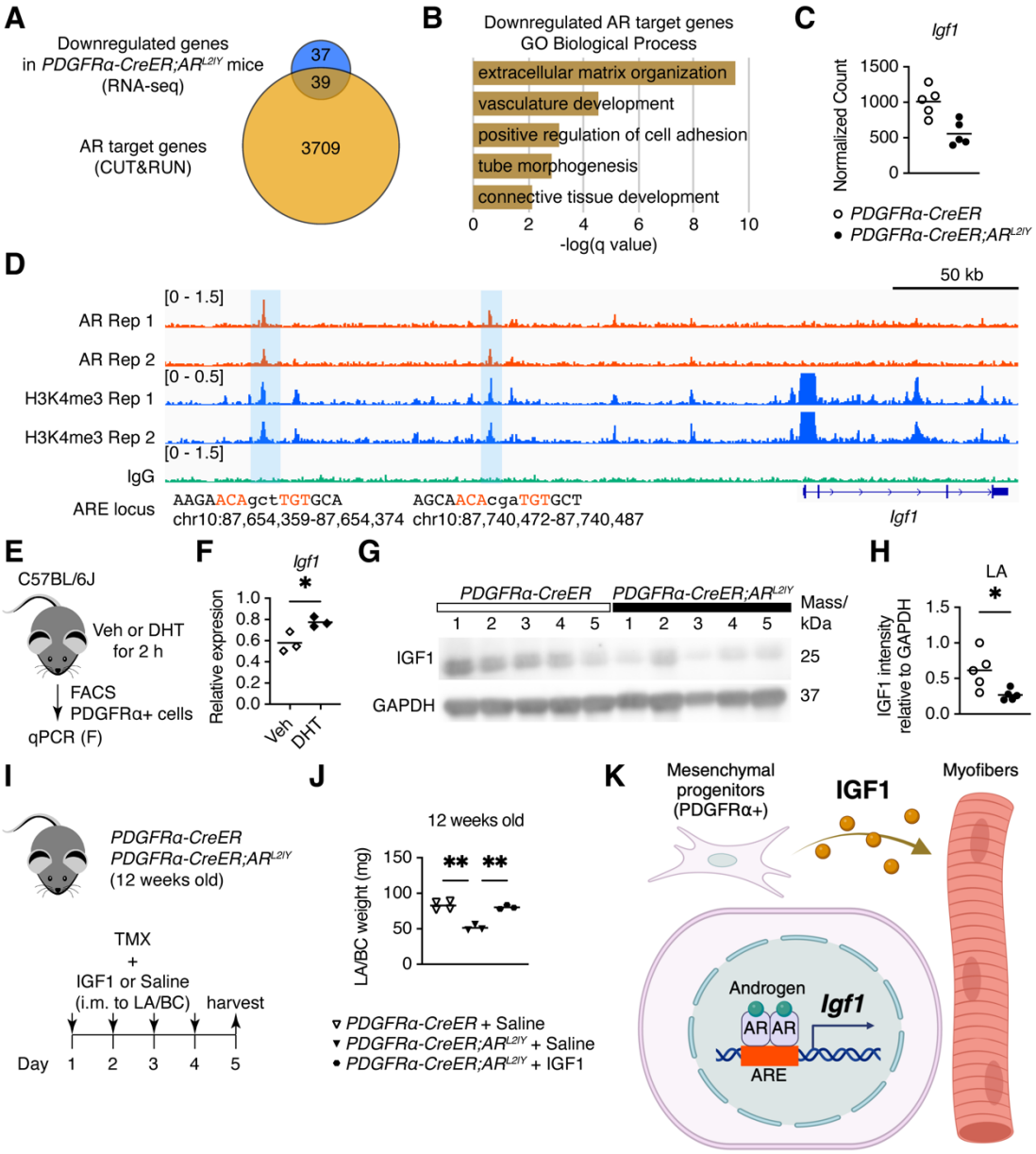

Figure 4. Regulation of *Igf1* in mesenchymal progenitors by AR. (A) Overlap of downregulated genes in PDGFRα+ cells from mutant mice and AR CUT&RUN peak-associated genes. (B) Top Gene Ontology (GO) Biological Process terms enriched within overlapped genes. (C) Normalized gene counts for *Igf1* obtained by RNA-seq. (D) AR and H3K4me3 CUT&RUN peaks with androgen response elements (ARE) at *Igf1* locus. The AREs are shown in red. Top left number is the y-axis range in counts per million (CPM). (E) Experimental design for qPCR

785 after treatment with dihydrotestosterone (DHT). (F) qPCR analysis of *Igf1* in PDGFRα+ cells
786 after DHT treatment (n = 3 mice/condition). Unpaired t-test with Welch's correction. (G and H)
787 Western blotting of IGF1 and GAPDH (G) and their quantification (H) in levator ani (LA)
788 muscles from control and mutant mice (n = 5). Unpaired t-test with Welch's correction. (I)
789 Experimental design for intramuscular injection (i.m.) of IGF1 to LA and bulbocavernosus (BC)
790 muscles, followed by tamoxifen (TMX) treatment and sample harvest in 12-week-old control
791 and mutant mice. (J) Mass of LA/BC muscles in saline- or IGF1-injected control and mutant
792 mice (n = 4 control, n = 3 mutant mice with saline or IGF1). Brown-Forsythe and Welch's
793 ANOVA test with Dunnett's T3 multiple comparison test: *$p < 0.05$, **$p < 0.01$. (K) Regulation
794 of *Igf1* by AR in mesenchymal progenitors of skeletal muscle. Created with BioRender.com.